

3. RESULTS

3.1. Human and mouse *OPA1* expression

3.1.1. Human and mouse tissues contain *OPA1* transcripts of different lengths

The human and mouse *OPA1* open reading frame (ORF) is 3 kb long. The 3'untranslated region (3'UTR) of the first described human (*h*) *OPA1* cDNA had a length of 3 kb, whereas the 3'UTR of the mouse *OPA1* (*m*) cDNA extended for around 1 kb. In order to test for additional transcript sizes, *OPA1* mRNA expression was analysed in human and mouse tissues by northern blot analysis. PolyA⁺-RNA isolated from various anatomical parts of the brain and tissues from both organisms was hybridised with radioactively labelled specific probes (Figure 7A). On human northern blots hybridisation revealed a pattern of 4 bands in all tissue samples tested. The detected transcripts had a length of 4, 5, 6 and 7 kb (Figure 7B and Figure 8). In contrast, on mouse northern blots a pattern of two transcripts of 4 and 7 kb was detected (Figure 9 upper panel). This raised the question whether all transcripts coded for all main protein domains of *OPA1*. In a follow-up experiment probes corresponding to the mitochondrial leader, the acidic, the coiled-coil 1 (CC1), the GTPase, the middle and the CC2 domain were generated from the *hOPA1* and the *mOPA1* cDNA. Since the same patterns of 4 (human) and 2 (mouse) bands appeared for all probes used, one can conclude that all transcripts, independent of their length, contained all the important domains of the *hOPA1* and *mOPA1* coding region. Of note, the *OPA1* mitochondrial leader sequence was detected in all *OPA1* mRNAs, which means that all the proteins translated from the different mRNAs are imported into mitochondria.

3.1.2. Steady-state levels of different *OPA1* transcripts vary in different tissues in both organisms

Northern blots of mouse tissues revealed different relative steady-state mRNA levels of the two *OPA1* transcript variants in the various tissues (Figure 9 upper panel).

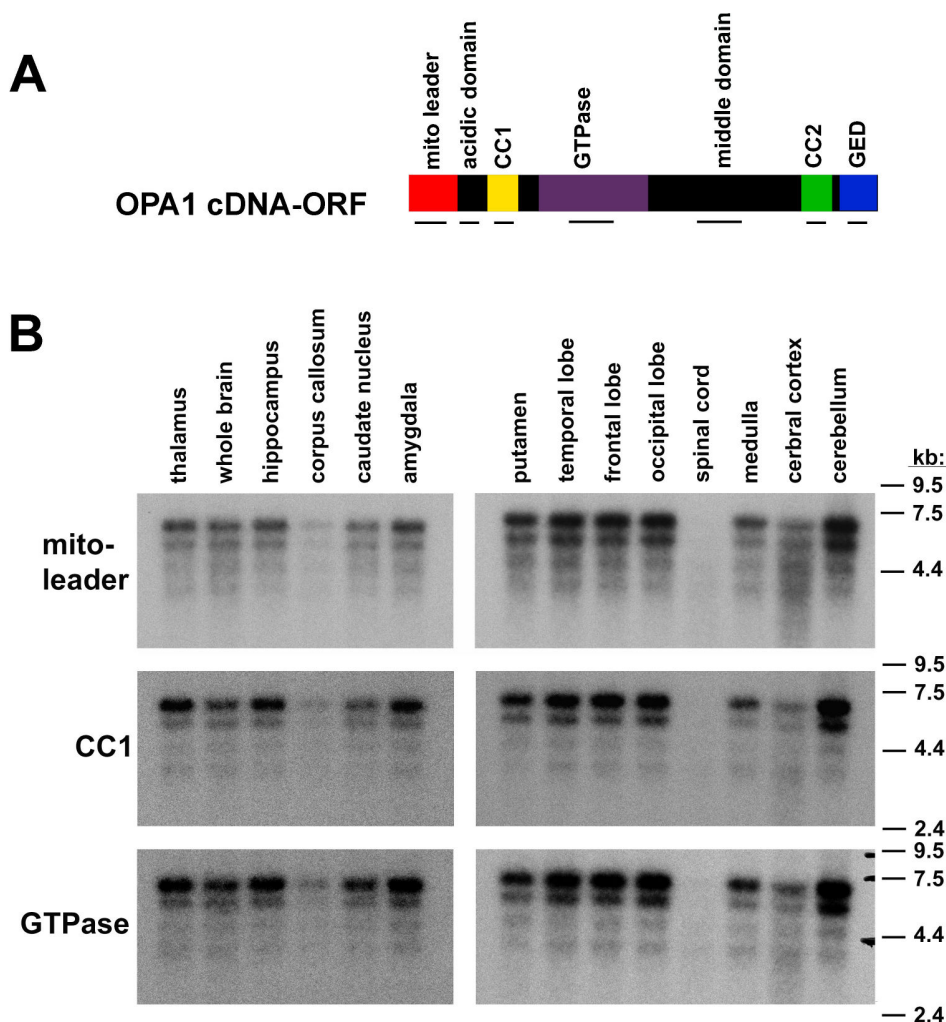


Figure 7. Northern blot analysis of human anatomical brain areas

(A) The graphic indicates the discrete functional protein domains of OPA1. The horizontal bars below the cartoon depict the different probes used in the hybridisation experiments. (B) Northern blot exposures of human polyA⁺-RNA isolated from various anatomical brain areas are shown after hybridisation with different probes corresponding to the mitochondrial leader, CC1 domain and GTPase domain of OPA1. The same four bands (4 kb, 5 kb, 6 kb, and 7 kb) are detected by the different probes used. The signals detected for the longer two transcript forms are stronger than for the two shorter transcripts.

The strongest signal for the short mRNA species relative to the long variant was observed in liver, followed by testis. In tissues like skeletal muscle, brain and heart, the situation was reverse with higher concentrations of the 7 kb transcript in comparison to the short 4 kb version. Signals detected in different lanes were not directly comparable since the loading of equal amounts of mRNAs could not be guaranteed. Further, a northern blot of mouse embryo mRNA of different developmental stages was hybridised with the same probes. The relative mRNA concentrations of both transcripts were constant for all samples revealing equally strong 4 and 7 kb bands for embryonic stages tested (Figure 9 upper panel).

The differences in relative mRNA steady-state levels in human tissue blots were not as prominent as in the mouse tissues. Still, slight differences in signal strength for the various transcript species could be noticed for different tissues (Figure 8). The signal strength, and therefore the abundance of the two longer transcripts were increased in comparison to the two shorter transcripts in the brain and ovary samples. Other tissues, like liver and pancreas showed higher abundances of the shorter transcripts, as also seen in the mouse liver and testis.

3.1.3. Analysis of polyadenylation signals in the human and mouse *OPA1* 3' untranslated region

Human *OPA1* gene expression results in 8 different splice variants. Three exons are alternatively spliced: 4 (108 bp), 4b (54 bp) and 5b (111 bp) (Delettre et al., 2001). These exons give rise to transcripts that differ in size by a maximum of 273 bp. This size difference does not explain the difference in length observed for *OPA1* transcripts on the northern blots described above. Therefore, the observed differences in transcript length have been attributed to the untranslated regions of the mRNAs. A differential usage of polyadenylation signals in the 3'untranslated region (3'UTR) was suspected. The presence and location of canonical polyadenylation sequence motifs in the *hOPA1* cDNA sequence were determined. The Unigene cluster Hs. 147946 for the *hOPA1* gene listed 276 ESTs that were downloaded from the NCBI web site (<http://www.ncbi.nlm.nih.gov>) and aligned using the LASERGENE software package. A consensus sequence for the *hOPA1* cDNA was created containing a 3'UTR of 3234 bp starting after the stop codon UAA of the *hOPA1* gene.

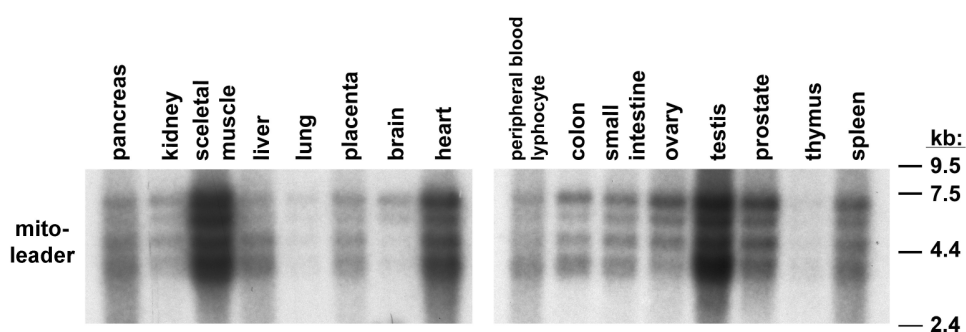


Figure 8. Tissue specific differential polyadenylation in human tissues

A representative hybridisation result of human multi tissue northern blots contains polyA⁺-RNA obtained with the *hOPA1* probes spanning functional domains, as depicted in Figure 7A. The hybridisation result with a probe corresponding to the mitochondrial leader sequence is shown. Identical results were obtained after hybridisation of probes corresponding to the other domains. Again, four bands were detected, however, compared to Figure 7 there was shift of signal strength towards the shorter bands in the tissues of inner organs, like liver and pancreas.

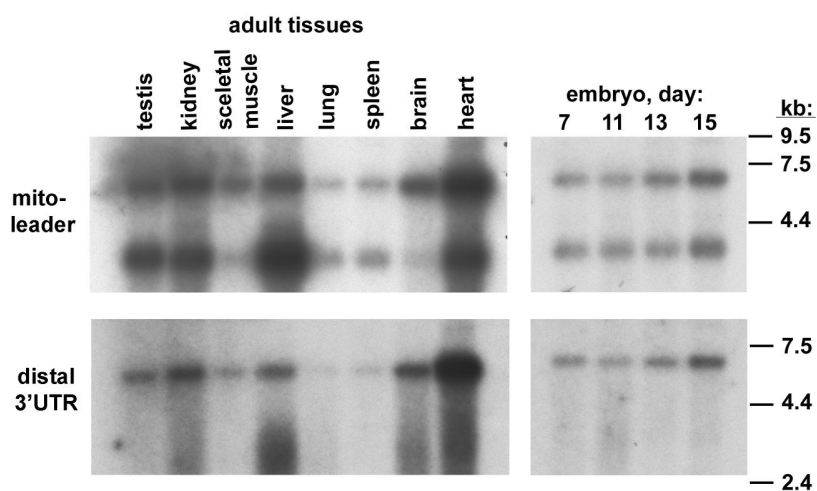


Figure 9. Tissue specific differential polyadenylation in mouse tissues

The hybridisation result of northern blots containing polyA⁺-RNA isolated from various adult and embryonic mouse tissues are shown. A probe corresponding to the mitochondrial leader sequence detected two bands of 4.0 and 7.0 kb. Identical results were obtained after hybridisation of probes corresponding to the CC1, GTPase, middle and CC2 domain. In testis, kidney and, most prominent in liver, the signal strength of the shorter band is markedly increased versus the signal of the longer transcripts. The opposite situation, higher abundance of the longer transcript cluster, is observed in tissues like skeletal muscle, brain and heart. The hybridisation result obtained for the mouse 3'UTR probe encompassing the distal conserved sequence element is shown in the lower panel. Here, only the long 7 kb band was detected. The probe that corresponded to the proximal part showed the same results as ORF-probes (upper panel).

This consensus 3'UTR extended the originally published full-length hOPA1 mRNA sequence by additional 308 bp. In this sequence, altogether 10 putative polyadenylation sites were identified. In most protein-coding genes, a conserved polyadenylation signal (AAUAAA) lies 10 – 30 nucleotides upstream from a poly(A) site where cleavage and polyadenylation occur. A GU- or U-rich sequence downstream from the poly(A) site contributes to the efficiency of cleavage/ polyadenylation (Lodish, 2004). A multiprotein complex carries out the cleavage and polyadenylation of a pre-mRNA. The exact location and sequence of the A-rich upstream element, the cleavage site, and the U-rich downstream element for each polyadenylation site is listed in Table 2. The absolute number of polyadenylated ESTs found for each cleavage site is also given. The polyadenylation sites were not evenly distributed over the 3'UTR but formed 4 clusters, separated each by 1 kb. mRNAs within one cluster could theoretically result in processed mRNAs differing in length by less than 290 bp. Assuming that mRNAs with such a length difference would appear as one band on the northern blots, it was concluded that the clusters represented groups of transcripts of ~4 kb, ~5 kb, ~6 kb and ~7 kb in length, correlating with the band pattern observed in the northern blot experiments.

Table 2. Human OPA1 polyadenylation sites and their position after the UAA stop codon

No.	A-rich sequence motif	Number of ESTs	Cleavage site	U-rich sequence motif
Cluster 1:				
1.	AAUAAA (107)	3	131	UGUAUGUU (135)
2.	AAUAAA (391)	1	415	UUGUUU (410)
Cluster 2:				
3.	AAUAAA (557)	1	977	GUGUUUU (1023)
4.	AAUAAA (1041)	2	1063	-
5.	AAUAAA (1135)	4	1157	GUUUUU (1161)
6.	AAUAAA (1625)	0	-	-
Cluster 3:				
7.	AAUAAA (2007)	9	2028	UGUAGUU (2047)
Cluster 4:				
8.	AAUAAA (2633)	2	2652	GGUUUUU (2655)
9.	AUUAAA (2907)	17	2928	UUUUUUU (2962)
10.	AUAAAA (3190)	9	3211	UUUUCAUU (3232)

Accordingly, polyadenylation signals for the mouse 3'UTR were analysed. The mouse Unigene database listed 85 ESTs for the *mOPA1* gene. The ESTs were downloaded and aligned with the ORF, in the same way as for the *hOPA1* sequences. The total length of the consensus sequence of this alignment was 3.8 kb which indicated that the mouse Unigene cluster did not represent the full-length mouse cDNA, since the northern blot analysis indicated the presence of a 7 kb transcript. By performing BLAST searches of the mouse EST division an additional number of 75 *OPA1* mouse ESTs were selected and added to the Unigene alignment. Now, the consensus sequence of *OPA1* cDNA had a length of ~7 kb including the virtual 3'UTR of 2.9 kb. Finally, using specific primers, the existence of this computationally predicted 3'UTR of the *mOPA1* cDNA was verified by RT-PCR (Figure 10). Bioinformatic examination of the entire mouse 3'UTR sequence identified only 4 canonical polyadenylation signals (Table 3). Based on the observations made for the *hOPA1* transcripts, *mOPA1* messages were expected to be processed at the two proximal sites to form a short cluster (4 kb), whereas the two remaining transcripts would be attributed to a cluster of longer transcripts (7 kb).

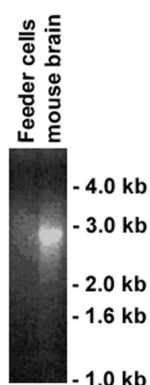


Figure 10. Verification of the *mOPA1* 3'untranslated region by RT-PCR

Total RNA extracted from Feeder cells and crude mouse brain extracts, taken from C57BL/6 mice, was used as template in an RT-PCR reaction. Mouse specific *OPA1* primers amplified the expected product of 2764 bp bridging the 3'UTR present in IMAGE clone AB044138 with the distal conserved sequence element in EST BQ175937.

Table 3. Mouse *OPA1* polyadenylation sites and their position after UAG stop codon

No.	A-rich sequence motif	Number of ESTs	Cleavage site	U-rich sequence motif
Cluster 1:				
1.	AAUAAA (111)	4	134	GUGUGUU (140)
2.	AAUAAA (369)	1	399	GUGUUCUGU (450)
Cluster 2:				
3.	AAUAAA (2584)	0	-	UGGUGUGU (2604)
4.	AUUAAA (2825)	7	2851	UUUGUUUU (2885)

In order to experimentally confirm the bioinformatic data, specific probes were generated complementary to the sequences upstream of each “polyadenylation cluster” as indicated in Figure 11A. The hybridisation results of human northern blots are shown in Figure 11B. As predicted, probe 4 detected only one band containing the longest transcripts of ~7 kb, probe 3 detected the two longest bands of ~6 kb and ~7 kb. Probe 2 hybridised to transcripts of clusters 2, 3 and 4, (~5 kb, ~6 kb and ~7 kb, respectively), and probe 1 resulted in the same band pattern as observed in the experiments using probes corresponding to the ORF (Figure 7).

Mouse northern blots revealed a similar picture. The radiolabelled probe of the *mOPA1* cDNA of the distal part of the 3'UTR hybridised only to the longer transcript of 7 kb, and the probe that corresponded to the proximal part detected both 4 and 7 kb mouse transcripts (Figure 9). Thus, the mouse *OPA1* mRNA populations result from usage of different polyadenylation sites.

Taken together, differential polyadenylation for both human and mouse transcripts was shown. For the human *OPA1* gene, four clusters of mRNA were identified, whereas in the mouse two such clusters exist.

3.2. Generation of *OPA1*-deficient mice

OPA1 gene expression is conserved in human and mouse tissues: the full-length ORF is expressed in all tissues examined, while differences were found only in the length of the 3'UTR. Further more, the human and mouse *OPA1* proteins show 98% identity. Based on these similarities, the mouse is genetically a good model system for studying the role of *OPA1 in vivo*.

3.2.1. Intron-Exon structure of the mouse *OPA1* gene

The mouse *OPA1* sequence was downloaded from the CELERA website. It extends over 100 kb and consists of 31 exons. The intron-exon organisation was determined by comparison of the murine *OPA1* cDNA with the genomic DNA sequence (Table 4).

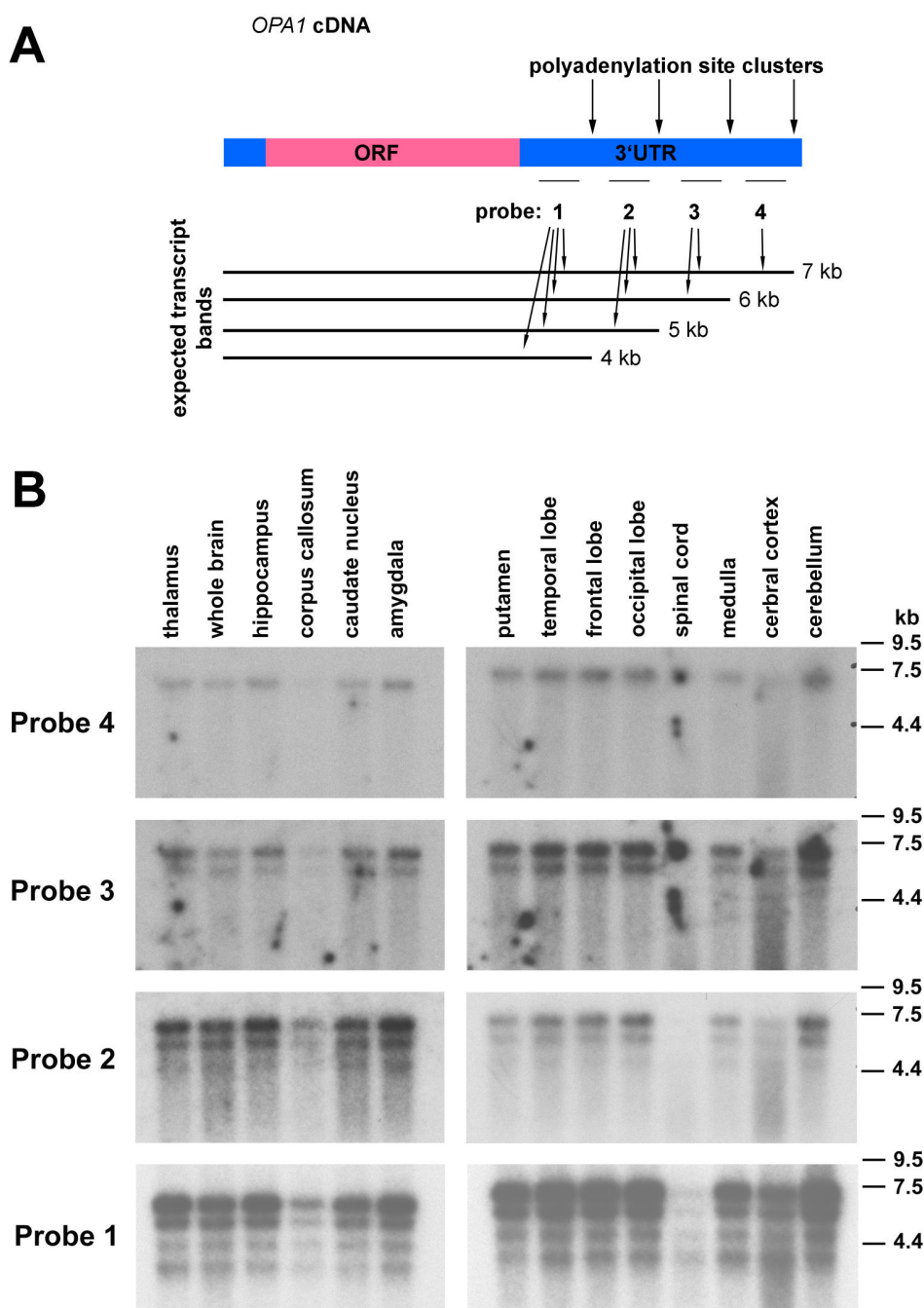


Figure 11. Northern blot analysis of human brain samples with probes of the 3'untranslated region of *hOPA1*

(A) The cDNA structure of *hOPA1* is given. Vertical arrows point at the location of the four polyadenylation site clusters in the *hOPA1* 3'UTR. Horizontal bars represent the probes 1, 2, 3, and 4 that correspond to specific upstream sequences for each cluster. Under each probe arrows point at expected transcript bands. (B) Hybridisation results of human brain northern blots containing polyA⁺-RNA from different brain parts are shown for the *hOPA1* 3'UTR probes 1, 2, 3, and 4. The four bands shown differ in the length of the transcript 3'UTR.

Table 4. Intron-Exon structure of the mouse *OPA1* gene with their lengths in base pairs and intron/exon and exon/intron borders

	INTRON	LENGTH in bp	BORDER IN/EX	EXON	LENGTH in bp	BORDER EX/IN
1.	1	NA*	GGAT	1	32	TGGT
2.	2	5412	AGTG	2	319	AAGT
3.	3	598	AGAC	3	97	GGGT
4.	4	1183	AGAG	4	108	AGGT
5.	4b	463	AGGT	4b	54	AGGT
6.	5	804	AGGT	5	68	AGGT
7.	5b	7940	AGGG	5b	111	AGGT
8.	6	4449	AGGT	6	54	AGGT
9.	7	3250	AGTT	7	105	AGGT
10.	8	2044	AGAA	8	87	GGGT
11.	9	583	AGGT	9	114	AGGT
12.	10	2143	AGGT	10	81	ATGT
13.	11	105	AGCT	11	75	AGGT
14.	12	467	AGAC	12	72	ACGT
15.	13	82	AGAC	13	100	AGGT
16.	14	256	AGAC	14	131	GGGT
17.	15	1926	AGAT	15	73	AGGT
18.	16	89	AGGA	16	73	AAGT
19.	17	851	AGGA	17	116	AGGT
20.	18	742	AGCC	18	65	GGGT
21.	19	643	AGAA	19	77	TGGT
22.	20	1433	AGGG	20	166	AGGT
23.	21	2078	AGGT	21	153	TGGT
24.	22	237	AGAG	22	109	TAGT
25.	23	585	AGCT	23	80	AGGT
26.	24	3922	AGTG	24	141	TGGT
27.	25	3095	AGAT	25	117	AGGT
28.	26	802	AGCT	26	94	AGGT
29.	27	364	AGTT	27	111	CAGT
30.	28	18728	AGAG	28	75	AAGT
31.	29	2678	AGAA	29	NA	NA

* NA stands for not available data.

3.2.2. Generation of the targeting vector

OPA1 mutations in most adOA patients are thought to result in haploinsufficiency. In order to best mimic this situation in mice, the *OPA1* gene expression was completely abolished. In addition, homozygous *OPA1* knockout mice would allow to study the effect of loss of *OPA1* for a cell and during development. In order to avoid residual expression of *OPA1* by alternative splicing of exons 4, 4b and 5b, a site located upstream of these exons was chosen for targeting. For the generation of the *OPA1* targeting vector a short and a long arm (2.2 kb and 5.5 kb, respectively), amplified by PCR, were cloned separately into the pGEM-Teasy vector. After that, the short arm was cloned into the XhoI and NotI restriction sites of the pTV.flox vector, followed by cloning of the long arm into the BamHI and Ascl sites. This resulted in the *neomycin* resistance gene cassette residing between the long and the short arm in 3'-5' orientation, replacing a part of exon 2 (Figure 12A). This intervention introduced a stop codon into exon 2, which destroyed the *OPA1*-ORF. A possible skipping of either exon 2 or exons 2 and 3 of the targeted allele would lead to a premature stop codon in exons 3 or 4, respectively.

3.2.3. Generation of mice lacking one *OPA1* allele

The 129/Ola ES-cell line was transfected with the linearised (NotI) pTV.flox-*OPA1* targeting vector through electroporation. This vector carried a *neomycin* resistance cassette, which is used for a negative-selection strategy. The clones that had undergone homologous recombination were identified using Southern blot analysis of the isolated genomic DNA (Chapter 3.2.4.). The first screening of 288 clones resulted in 4 positive ES-cell clones. These clones were used to produce chimeric mice by blastocyst injection. In order to test chimeric mice for germ line transmission they were crossed with C57BL/6 animals (black fur colour), the donor strain of the blastocyst. The ES cells were obtained from 129/Ola mice, a mouse strain with chinchilla fur colour. If the ES cells incorporated into blastocysts and produced germ cells, the offspring of crossed animals could be distinguished by the colour of their coat, which should be brown. Three out of four positive clones injected gave chimeric offspring, but germ line transmission was accomplished only with clone number 2 in only two out of four animals, even with two repeated injections. Germ-line transmission of the targeted allele was confirmed by

PCR-genotyping of brown offspring (Figure 15B). PCR-genotyping of DNA isolated from tail biopsies determined the genotype of brown-coloured F1 mice. Crossing of two heterozygous F1 mice led to the F2 generation, which included wild-type and heterozygous mice, as determined by PCR-genotyping. Homozygous mice were never born from these intercrosses.

3.2.4. Confirmation of the knockout event

ES clones were tested for homologous recombination by Southern blot analysis of the MfeI restriction enzyme-digested DNA of each clone. Hybridisation with a genomic probe, as presented in Figure 12A, resulted in DNA bands of 4.9 and 6.1 kb length for clones with homologous recombination versus only a 4.9 kb band for clones in which homologous recombination had not taken place (Figure 12B). Positive clones were then confirmed using PCR-genotyping (Figure 12C).

In order to confirm loss of OPA1 protein in homozygous mutant mice western blot analysis was performed with proteins isolated from mouse embryonic fibroblasts (MEFs) generated by SV40 (large T)-transformation by our collaborator D. C. Chan. OPA1^{-/-} MEFs did not contain detectable levels of OPA1 protein, whereas in wild-type cells detection was possible (Figure 12D). This indicated that functional gene expression of OPA1 from the mutant allele was completely abolished.

3.3. Phenotypic analysis of heterozygous *OPA1* knockout mice

All animals used for phenotypic analysis were either of mixed C57BL/6 and 129/Ola backgrounds (F1) or of pure 129/Ola background. OPA1 heterozygous mice of either background were born at expected Mendelian ratio (Table 5). They were viable and fertile, while OPA1^{-/-} animals were not detected among the offspring of crosses of OPA1^{+/-} mice of a mixed C57BL/6/129/Ola genetic background. In order to investigate if haploinsufficiency happens at the protein level in OPA1^{+/-} mice, western blot analysis of tissues taken from heterozygous and wild-type mice was performed. The amount of protein was, indeed, reduced in the heterozygous mice as compared to wild-type mice in liver and brain (Figure 13A).

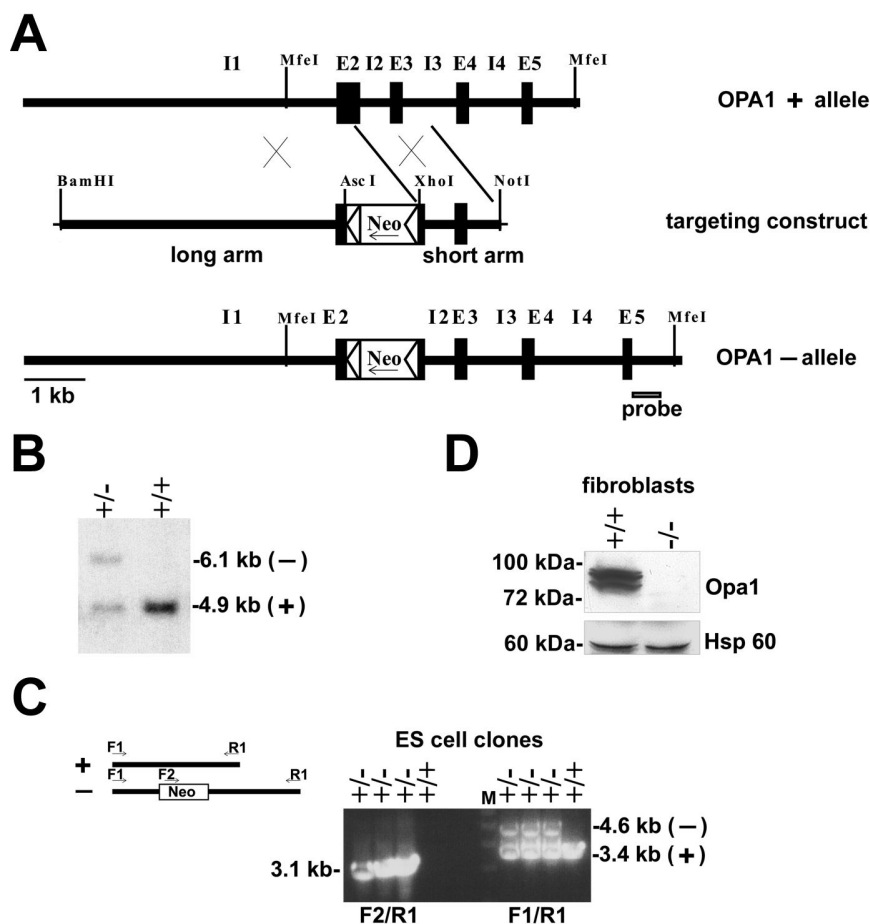


Figure 12. Construction of knockout mice and confirmation of the targeting event

(A) Genomic targeting of *OPA1*. *OPA1*⁺ indicates the wild-type *OPA1* genomic locus with exons (E) and introns (I) and *OPA1*⁻ the targeted allele. Homologous recombination results in the substitution of a part of exon 2 (E2) with a *neomycin* resistance cassette (Neo) and a premature stop codon in exon 2. Enzymes used for cloning are marked (BamHI, AscI, XhoI, NotI). NotI was used for linearisation. The arrow in the *neomycin* cassette indicates the 5'-3' orientation of the gene. (B) Southern blot analysis of G418 resistant clones was used to distinguish between wild-type cells (+/+) and cells with homologous recombination (+/-). Genomic DNA was digested with MfeI and analysed with the probe indicated in A. (C) PCR-genotyping of three G418-resistant clones. Three primers labelled F1, F2 and R1 were used in two separate reactions to amplify distinct fragments from the wild-type (+) and knockout (-) loci. (D) Western blot analysis of wild-type (+/+) and *OPA1*-deficient (-/-) mouse embryonic fibroblasts. Lysates were analysed with mouse monoclonal antibodies directed against *OPA1* and HSP60.

Table 5. Genotyping of newborn pups and different staged embryos on hybrid C57BL/6/129/Ola background

Stage	Total	+/+	+/-	-/-
Newborn	445	150	295	0
E12.0	24	8	16	0
E10.0	14	5	9	0
E9.0	23	8	15	0
E8.5	49	13	30	6*
E7.5	146	34	76	36
E6.5	41	10	21	10

*3 partially resorbed embryos

3.3.1. OPA1^{+/-} mice contain reduced levels of mitochondrial DNA

It had been previously reported that cell lines obtained from adOA patients showed decreased mtDNA levels (Kim et al., 2005). In order to test if OPA1 heterozygous mice also contain reduced levels of mtDNA compared to their wild-type littermates, quantitative PCR was performed. Indeed, mtDNA levels in all OPA1^{+/-} tissues examined were reduced: 32% reduction of wild-type level in brain, 20% in liver and 19% in retina (Figure 13B).

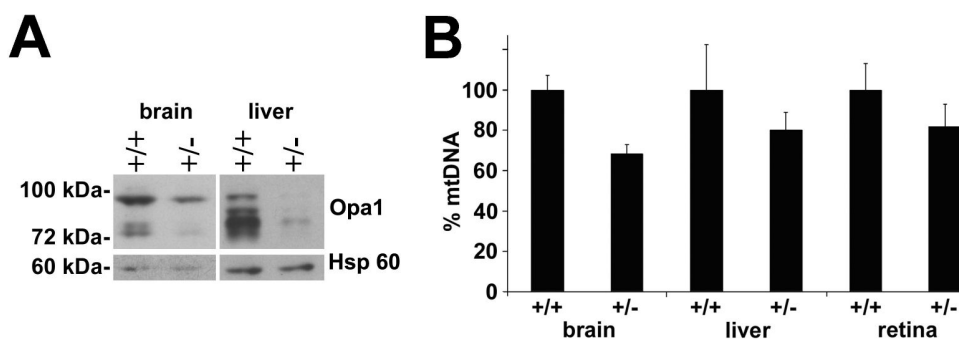


Figure 13. Analysis of OPA1^{+/-} versus OPA1^{+/+} mice

(A) Western analysis of brain and liver lysates of heterozygous (+/-) versus wild-type (+/+) animals. Lysates were analysed with mouse monoclonal antibodies directed against OPA1 and HSP60. (B) Decreased mitochondrial DNA (mtDNA) levels in tissues of heterozygous OPA1-deficient mice. The relative value of mtDNA was determined for adult mouse organs using quantitative (real-time) PCR. The relative value was obtained by dividing mtDNA amount by chromosomal DNA amount. The values are indicated as percentage of the mean levels of the relative mtDNA amounts in wild-type specimen. n=3. All bars indicate mean \pm SD.

3.3.2. Histological examination of the retina and the optic nerve

Phenotypic analysis of heterozygous mice was performed on the visual system, which had been previously described to be affected in adOA patients. Tissue sections of retinæ of wild-type and OPA1 heterozygous knockout mice of different ages starting from postnatal day 1 till 12 months old animals were cresyl-violet stained and observed under the light microscope. Retinæ of each animal examined showed a normal organisation and thickness of all retinal layers. A loss of cells or any sign of degeneration was never observed in OPA1^{+/-} mice (Figure 14A).

Additionally, the optic nerve was examined. In wild-type mice the myelination of the optic fibres is detectable within the first 7 days after birth (Foran and Peterson, 1992). Cresyl-violet stained sections of optic nerves would, therefore, reveal if decreased OPA1 protein levels had an influence on myelination of these nerves. The thickness of myelin sheaths, as well as axon numbers in the OPA1^{+/-} mice were however, comparable to wild-type mice (Figure 14B).

Electron microscopic images of transversal sections of optic nerves are often used in order to test if any change in axonal organisation, thickness of myelin, loss or gain of myelin sheets took place. Using this method, it is also possible to observe changes in the ultra-structure of axonal mitochondria, which are known to play an important role at synapses (Li et al., 2004; Rowland et al., 2000; Shepherd and Harris, 1998). Mice of different ages (from post-natal day (P) 1 to 12 months old) were examined for such changes in optic nerves. Optic nerves of all OPA1^{+/-} animals had normal axonal and myelin organisation. Furthermore, their mitochondria had the same morphology as wild-type mitochondria (Figure 14C).

3.4. Phenotypic analysis of homozygous OPA1 knockout mice

To completely knockout OPA1 function, OPA1^{-/-} mice were produced by intercrossing of OPA1^{+/-} mice of a C57BL/6/129/Ola background. Hence, the genetic background of heterozygous and homozygous OPA1-deficient mice was the same.

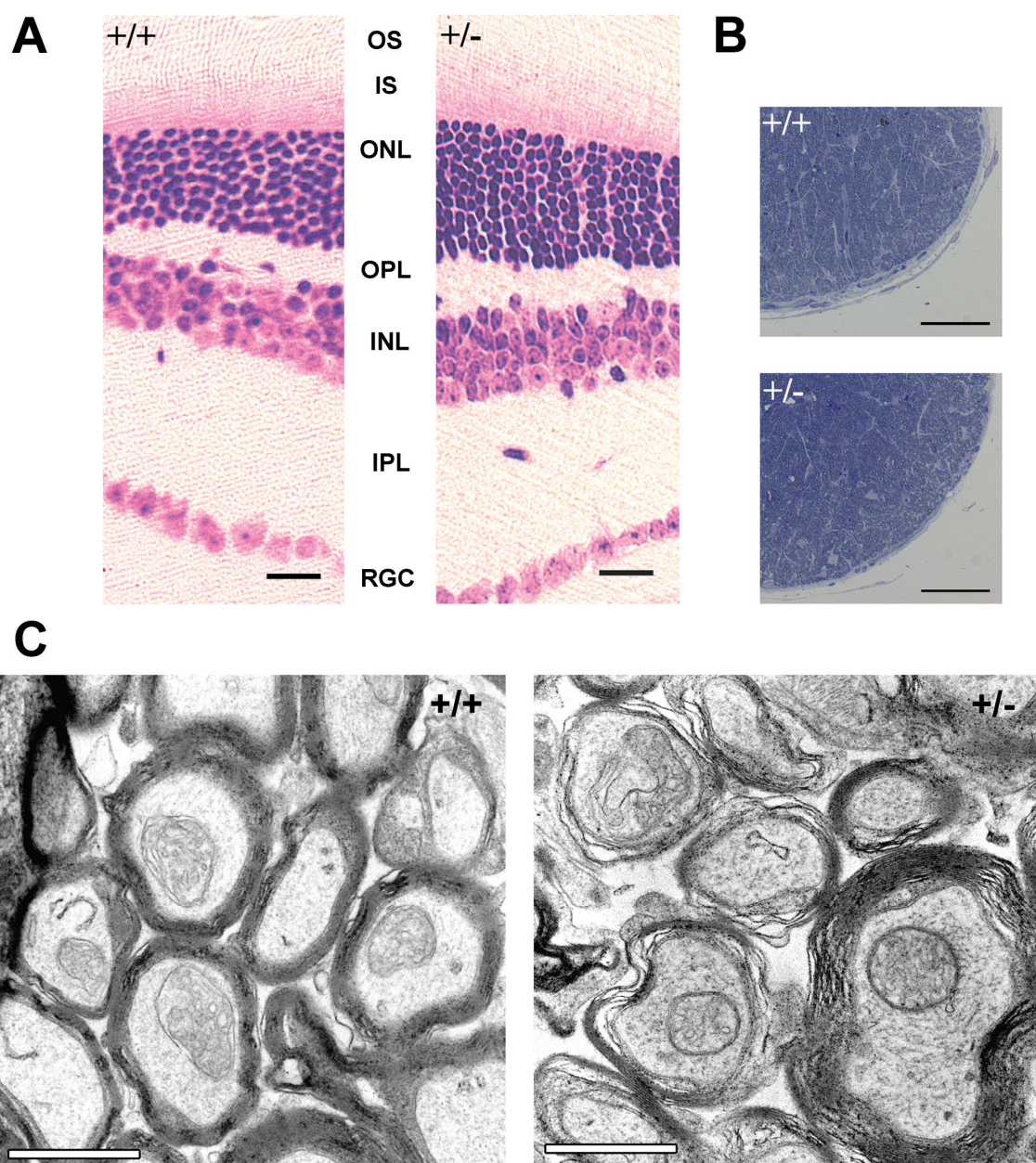


Figure 14. Histological analysis of OPA1^{+/-} versus OPA1^{+/+} mice

(A) Cresyl-violet staining of retinal sections from wild-type (+/+) and heterozygous (+/-) three months old mice show no difference. OS= outer photoreceptor segments; IS= inner photoreceptor segments; ONL= outer nuclear layer; OPL= outer plexiform layer; INL= inner nuclear layer; IPL= inner plexiform layer; RGC= retinal ganglion cell layer. Scale bars: 50 μ m. (B) Cresyl-violet staining of optic nerve sections from the same mice as in A show no difference between wild-type and heterozygous mice. Scale bars: 50 μ m. (C) Electron micrographs of transverse sections of optic nerves presented in B. Optic nerves and mitochondria of wild-type mice do not differ from those of OPA1 heterozygous knockout mice. Scale bars: 1 μ m.

3.4.1. Loss of OPA1 causes early embryonic lethality

OPA1^{-/-} mice were never observed to be born from intercrosses of heterozygous animals (Table 5). In order to determine the precise time-point of death of OPA1^{-/-} mice, embryos of different developmental stages were isolated and genotyped by PCR (Figure 15A). No OPA1^{-/-} embryos were found at embryonic days E12, E10 and E9 (Table 5). At E8.5, few severely retarded embryos and remnants of resorbed embryos were detected (Table 5). Starting from day E6.5, all OPA1^{-/-} embryos were considerably smaller in size than their wild-type or heterozygous littermates (Figure 15B). OPA1^{-/-} embryos reached day E7.5 with normal Mendelian frequencies, but at E8.5 most of them were resorbed. This analysis revealed that OPA1^{-/-} embryos pass through blastular stages but die during early gastrulation (Theiler stage 10). Therefore one can conclude that OPA1 is absolutely required for embryonic development beyond E8.5.

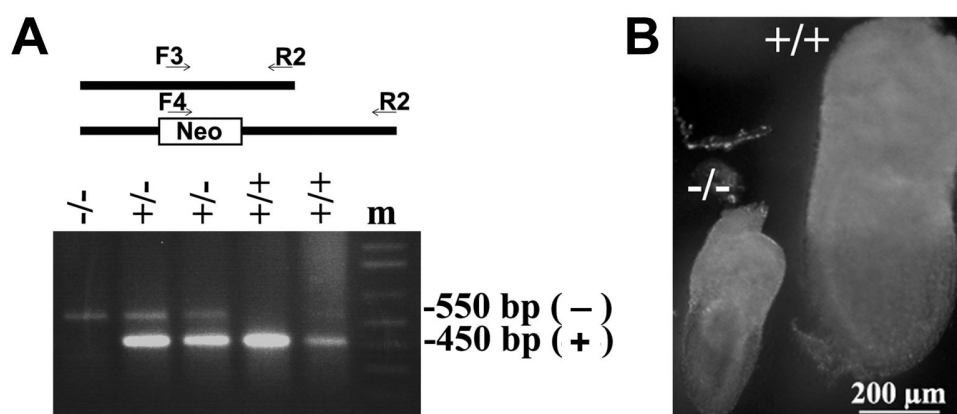


Figure 15. Analysis of OPA1 deficient embryos

(A) PCR-genotyping of embryos or mice. Three primers (F3, F4 and R2) were used simultaneously to distinguish between wild-type (+/+), heterozygous (+/-) and homozygous OPA1-deficient (-/-) embryos. m: molecular weight marker. (B) Morphology of wild-type (+/+) versus homozygous OPA1-deficient (-/-) E7.5 embryos. Note that the OPA1-deficient embryo is much smaller than its wild-type littermate.

3.4.2. OPA1^{-/-} embryos have fragmented mitochondria

OPA1 is thought to play a role in the fusion of mitochondria (see introduction) and *in vitro* experiments have shown that loss of OPA1 leads to their fragmentation (Chen et al., 2005; Griparic et al., 2004; Olichon et al., 2003). To examine the effect of the complete loss of OPA1 on mitochondrial morphology during embryogenesis, E7.5 embryos were stained immediately after isolation with MitoTracker Red. This dye allows

staining of mitochondria due to their membrane potential. Observation of stained embryos under a confocal microscope revealed differences in mitochondrial morphology between wild-type and knockout embryos: *OPA1*^{-/-} embryos contained only vesicular-shaped mitochondria, indicative for a complete fragmentation of the mitochondrial network (Figure 16C and F). In contrast, wild-type embryos showed mainly tubular-shaped mitochondrial networks (Figure 16A and D). Interestingly, heterozygous embryos contained a heterogeneous population of fragmented and extended mitochondria, though most of them were tubular-shaped as in the wild-type embryos (Figure 16B and E).

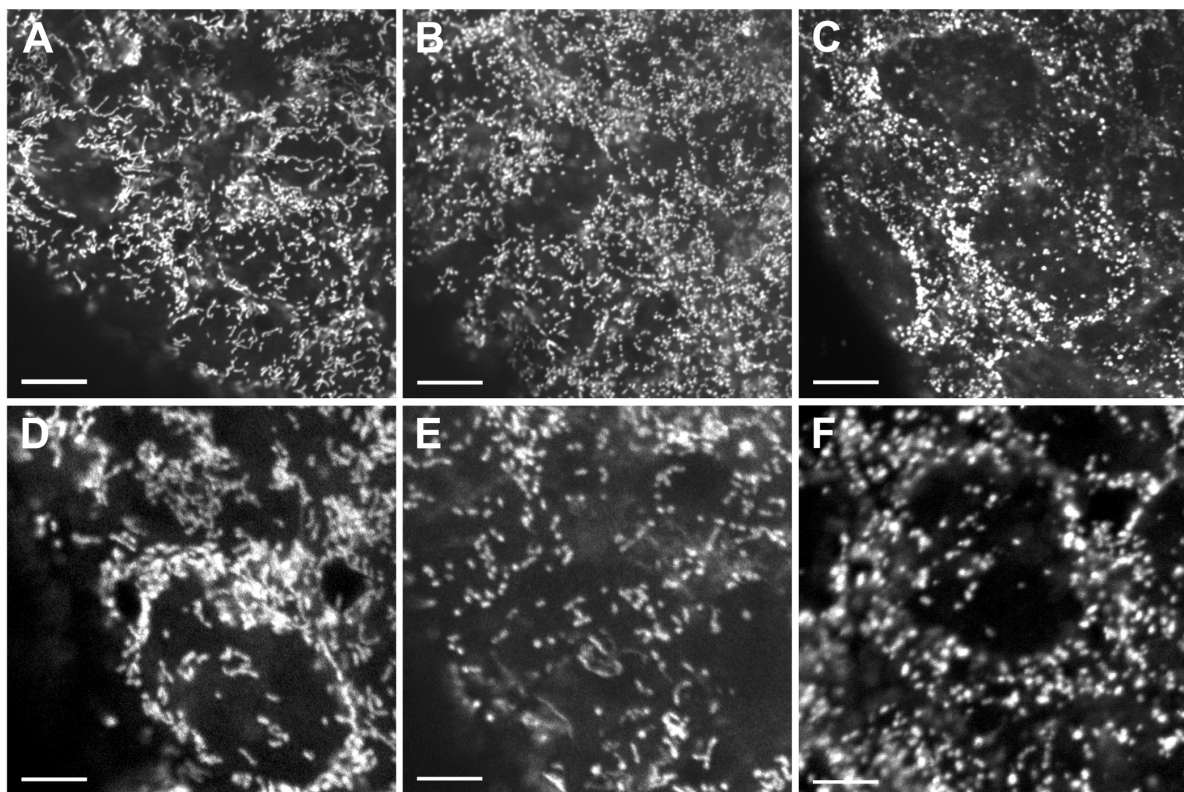


Figure 16. Morphological alterations in mitochondrial networks of mouse embryos

Mitochondrial morphology in wild-type (A and D) versus heterozygous (B and E) and homozygous mutant (C and F) E7.5 embryos. Note that in *OPA1*^{-/-} embryos all mitochondria are fragmented and that *OPA1*^{+/-} embryos have a heterogeneous population of fragmented and tubular mitochondria. The mitochondria were stained with MitoTracker Red. Scale bars in upper panel: 10 μ m; in lower panel: 5 μ m.

3.4.3. OPA1^{-/-} embryos contain reduced level of mitochondrial DNA

OPA1^{+/-} mice show reduced levels of mitochondrial (mt) DNA (Figure 13B). In order to explore the loss of mtDNA in OPA1^{-/-} embryos, quantitative PCR was performed on DNA preparations of embryos of different stages. In E6.5 mutant embryos, a slight decrease in mtDNA levels was noticed when compared to wild-type animals. OPA1^{+/-} embryos contained 95% and OPA1^{-/-} embryos 80% of wild-type mtDNA amounts (Figure 17 left panel). For day E7.5, the decrease in mtDNA levels was larger: 85% of wild-type mtDNA level in heterozygous and 60% in homozygous mutant embryos (Figure 17 right panel). Since littermate embryos differ slightly in their developmental stage, there was a natural variation in the mtDNA levels of different embryos. Nevertheless, a decrease in mtDNA levels was observed in all mutant embryos.

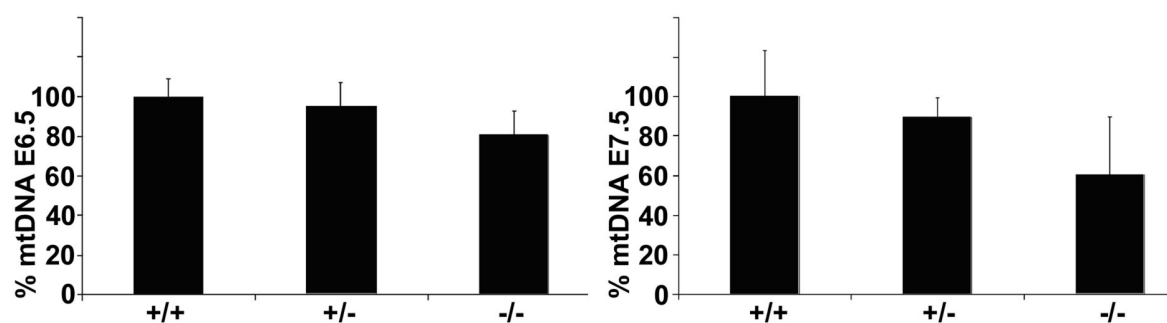


Figure 17. Decreased mtDNA levels in OPA1-deficient embryos

The relative amount of mtDNA was determined for E6.5 and E7.5 embryos using quantitative (real-time) PCR. The relative value was obtained by dividing the mtDNA amount by the chromosomal DNA amount. The values are indicated as percentage of the mean levels of the relative mtDNA amounts in wild-type specimen. The graphs summarize all embryonic data. n(E6.5 +/+)=3. n(E6.5 +/-)=7. n(E6.5 -/-)=4. n(E7.5 +/+)=5. n(E7.5 +/-)=8. n(E7.5 -/-)=5. All bars indicate mean \pm SD.

3.4.4. OPA1^{-/-} embryos show massive cell death at embryonic day 7.5

Various events leading to apoptosis focus on mitochondria, including the release of caspase activators like cytochrome c (Cai et al., 1998; Green and Reed, 1998; Liu et al., 1996; Reed, 1997), changes in electron transport, loss of mitochondrial transmembrane potential, altered cellular redox condition and participation of pro- and antiapoptotic Bcl-2 family proteins (reviewed in Danial and Korsmeyer, 2004; Green and Reed, 1998; Wang,

2001). Furthermore, cytochrome c release of mitochondria seems to be accompanied, or probably slightly preceded, by the fragmentation of mitochondria in HeLa cells (Arnoult et al., 2005; De Vos et al., 1998; Desagher et al., 1999; Frank et al., 2001; Karbowski et al., 2002; Karbowski and Youle, 2003; Zhuang et al., 1998). Since the OPA1-deficient embryos showed fragmented mitochondria, reduced size and resorption at E8.5, they were examined for signs of programmed cell death using the TUNEL assay. Cells that stained TUNEL-positive were those in which DNA degradation had occurred. Abundant TUNEL-positive staining was detected in E7.5 homozygous knockout embryos (Figure 18A lower panels), which was completely absent in heterozygous mutants and wild-type embryos (Figure 18A upper panels). Since DNA degradation also happens in necrotic cell death, electron microscopic studies of embryo sections were performed. It has been previously described that in cells undergoing apoptosis many events on the ultrastructural level take place: chromatin condensation around the periphery of the nucleus and appearance of various vesicles (Zhang et al., 1999). These vesicles sometimes appear to be releasing their content into the extracellular matrix; some of them are lysosomal-like. The cells of OPA1^{-/-} embryonic tissue, especially in the embryonic mesoderm, were loosely connected with increased chromatin condensation and various vesicles resembling those described above (Figure 18B). This is a clear indication for apoptotic cell death. Heterozygous and wild-type embryos showed closely packed cell structures and no signs of chromatin condensation and vesicle formation.

3.4.5. Fragmented mitochondria in OPA1^{-/-} cells

To further examine mitochondrial morphology in OPA1 null mutants, SV40-transformed mouse embryonic fibroblasts (MEFs) were generated from OPA1 wild-type and homozygous embryos in the laboratory of D. C. Chan. As expected, OPA1^{-/-} MEFs did not contain detectable levels of OPA1 protein on western blots (Figure 12D). In order to study their mitochondria in more detail, OPA1^{-/-} MEFs were stained with MitoTracker Green and compared to OPA1^{+/+} MEFs. All OPA1^{-/-} cells displayed severely fragmented mitochondrial networks (Figure 19B), as observed in the OPA1^{-/-} embryos (Figure 16). In contrast, wild-type cells displayed tubular-shaped mitochondria (Figure 19A).

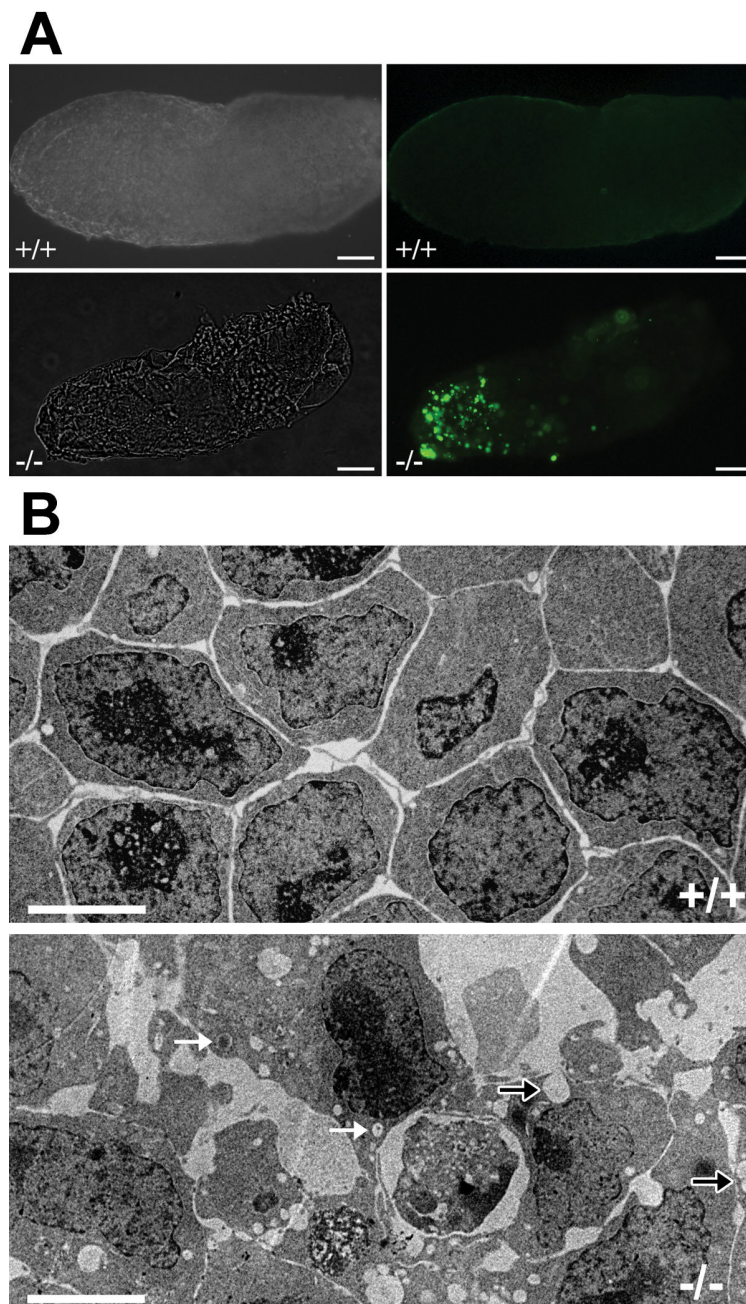


Figure 18. Analysis of apoptosis in OPA1-deficient embryos

(A) TUNEL staining (right panels) of whole-mount littermate E7.5 embryos shows abundant TUNEL-positive cells in $OPA1^{-/-}$ embryos. Left panels are phase contrast images. Scale bar: 100 μm . (B) Electron micrographs of transverse sections of wild-type (+/+) versus $OPA1^{-/-}$ E7.5 embryonic mesoderm. In $OPA1^{-/-}$ embryos, cells are loosely attached, chromatin is condensed and many vesicles, some of which are releasing their content into the extra cellular matrix (black arrows), and lysosomal-type vesicles (white arrows) are present. Scale bars: 5 μm .

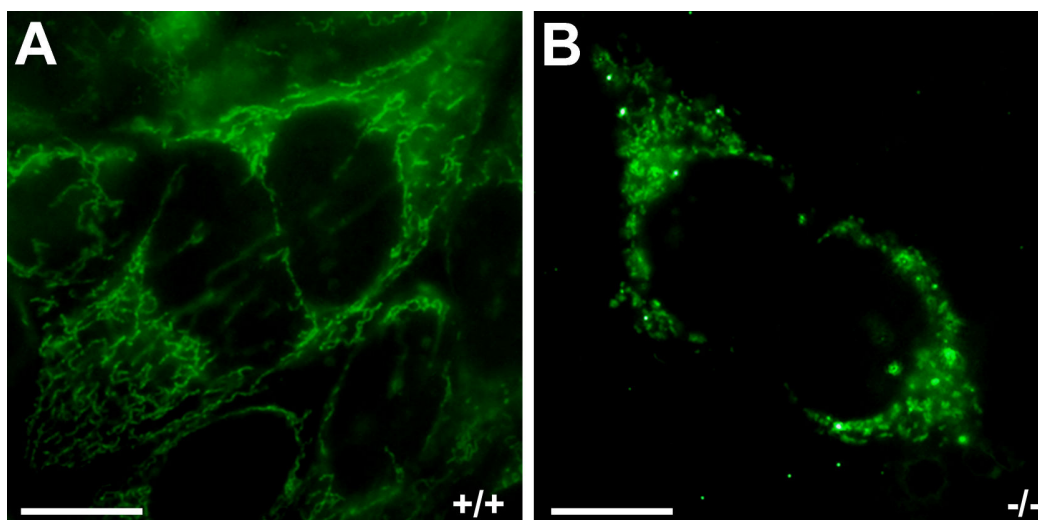


Figure 19. Mitochondrial fragmentation OPA1-null mouse embryonic fibroblasts (MEFs)

Image of MitoTracker Green-stained wild-type (A) and OPA1-null (B) MEFs. Note that in OPA1^{-/-} MEFs (B) all mitochondria are fragmented, whereas in OPA1^{+/+} cells (A) all mitochondrial are tubular. Scale bar: 10 μ m.

3.4.6. Ultrastructural changes of mitochondria in OPA1^{-/-} cells

Extremely fragmented mitochondria in OPA1^{-/-} embryos and MEFs led to assume further abnormalities in mitochondrial morphology. In order to study their morphology on an ultrastructural level, electron microscopy (EM) was performed. Mitochondria of wild-type MEFs had orderly arranged double membranes and long cristae that traversed almost through the entire matrix space (Figure 20 A and C). In contrast, most OPA1^{-/-} mitochondria contained completely disorganised double membranes and rudimentary cristae (Figure 20B and D). The mitochondrial membranes in OPA1^{-/-} cells divided the matrix like single septae or formed round-shaped bubbles. These bubbles resembled mitochondrial cristae that had lost their attachment to the rest of the inner membrane. Interestingly, all inner membranes were still tightly associated to each other like in wild-type cells; no broadening of cristae was noticed.

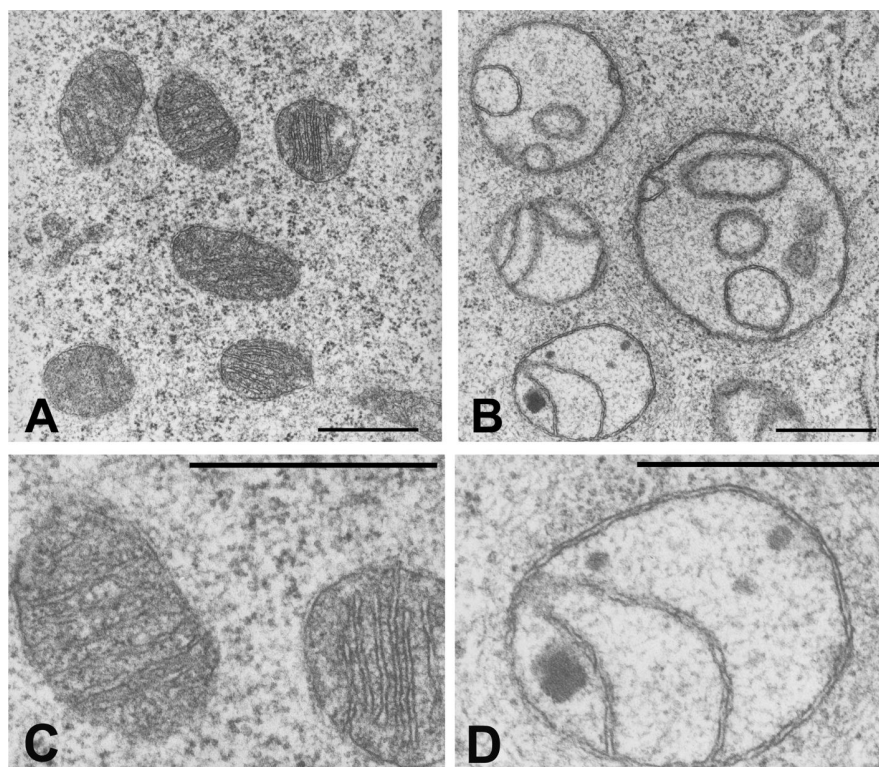


Figure 20. Electron micrographs of mitochondria of mouse embryonic fibroblasts

(A and C) Wild-type and (B and D) mutant mitochondria. $OPA1^{-/-}$ cells contain enlarged mitochondria with disorganized cristae. Scale bars: 1 μm .

3.4.7. $OPA1^{-/-}$ cells are respiration deficient

Knowing that respiratory chain complexes reside in mitochondrial cristae, the dramatic changes in mitochondrial ultrastructure were highly suggestive to affect respiratory chain function. Therefore, the amount and activity of the respiratory chain complexes were tested. First, total protein extracts of $OPA1^{+/+}$ and $OPA1^{-/-}$ cells were compared for the presence of components representative for the respiratory chain complexes on western blots. They were tested with antibodies directed against subunits of complex I (NADH-dehydrogenase; 39 kDa subunit), complex II (succinate dehydrogenase, SDH; 70 kDa subunit), complex IV (cytochrome c oxidase, COX; subunit I) and complex V (ATP synthase; subunit β). The amount of complex I was severely reduced in $OPA1^{-/-}$ cells and complex II showed a minor reduction. All other complexes

tested were found to be present at normal protein-expression levels (Figure 21A). In order to analyse if respiratory chain complexes were functional, thin sections of MEF-cell pellets were treated with substrates specific for complexes II and IV: succinate for complex II and cytochrome c for complex IV. In addition, either 4-nitrobluetetrazoliumchlorid (NBT) or 3,3'-diaminobenzidine (DAB) were used as indicators in order to monitor the activity of the respective complexes by changing their colour depending on the redox state of the dye. Isolated mitochondrial complex I activity cannot be determined on cryosections because NADH-dehydrogenases also exist in the cytoplasm. Complex II activity was found to be normal in knockout cells (Figure 21B upper panels). In contrast, enzyme histochemical staining for complex IV showed no activity in knockout cells, while wild-type cells showed usual brown staining (Figure 21B lower panels). Complex IV demonstrated not to be functional although western blot analysis indicated normal levels of subunit I of complex IV. This complex is comprised of 13 subunits, and antibodies are not available for all of them. It remains to be clarified if OPA1 isoform 1 plays a direct role in controlling complex IV activity or stability. Alternatively, the drastic changes in morphology and the reduced surface of the inner mitochondrial membrane in OPA1^{-/-} cells might affect the activity of complex IV in a more pronounced manner than the function of complex II.

Cytochrome c is a crucial component of the respiratory chain, functioning as an electron shuttle between complex III and complex IV of the respiratory chain (Lodish, 2004). It is localised in mitochondrial cristae and the intermembrane space. Since OPA1^{-/-} MEFs suffer from respiration deficiency, lack of cytochrome c could have contributed to the block of respiration. Western blot analysis of total protein extracts did not show any difference in amounts of cytochrome c between OPA1 wild-type and knockout cells (Figure 21A). Besides, cytochrome c immunostaining showed mitochondrial localisation in knockout cells as also seen in wild-type cells (Figure 23C).

An inefficient respiratory chain often leads to a reduction of the mitochondrial membrane potential ($\Delta\Psi_m$). The fusion of mitochondrial membranes proved to depend on this membrane potential. Since OPA1^{-/-} MEFs showed reduced respiration and fragmented mitochondria, their membrane potential was measured. The mitochondrial membrane potential is mainly generated by proton pumping of the respiratory chain complexes (Malka et al., 2005; Meeusen et al., 2004). JC-1 (5,5',6,6'-tetrachloro-1,1',3,3'-tetraethyl-benzimidazolo carbocyanine iodide) is a mitochondrial dye that accumulates in the matrix of intact mitochondria and forms red fluorescent aggregates. Dissipation of

$\Delta\Psi_m$ is reflected by a dissociation of JC-1 into monomers and dispersion over the entire cell combined with an alteration of its fluorescent emission properties towards green. This dye was used to compare $\Delta\Psi_m$ of OPA1^{+/+} and OPA1^{-/-} cells. Indeed, more than half of OPA1^{-/-} cells showed loss of $\Delta\Psi_m$ (Figure 22) when compared to wild-type cells. This change was even more pronounced in the presence of the ionophore valinomycin (Figure 22). This demonstrates that the mitochondrial membrane potential of OPA1^{-/-} fibroblasts is markedly reduced.

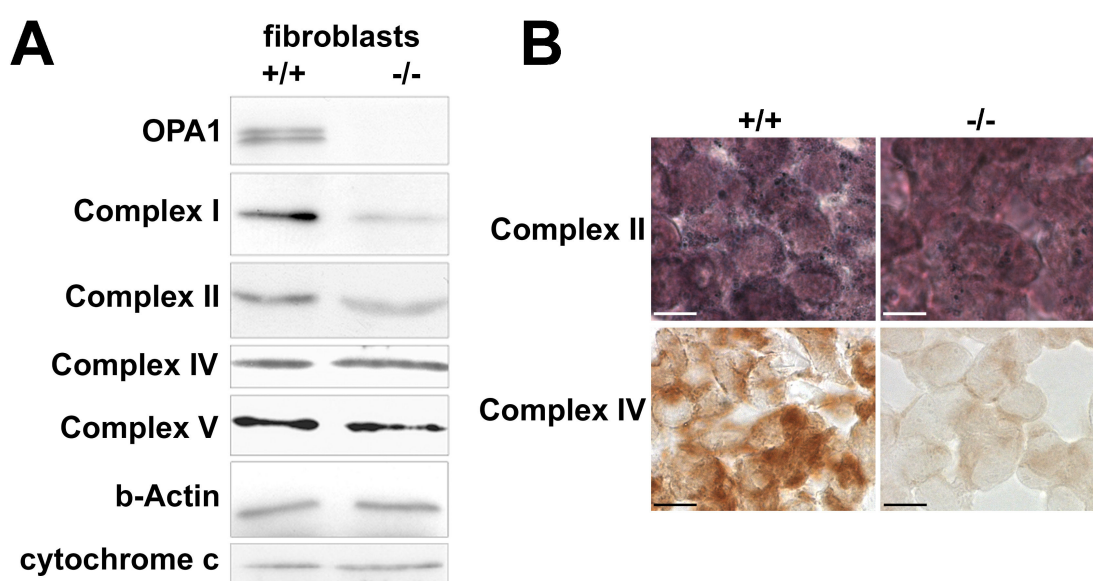


Figure 21. OPA1-deficient mouse embryonic fibroblasts show reduced respiration

(A) Presence of respiratory chain complexes in wild-type (+/+) and OPA1-deficient (-/-) mouse embryonic fibroblasts by immuno-blotting. Whole cell lysates were analysed with mouse monoclonal antibodies directed against OPA1, NADH-dehydrogenase (Complex I), succinate-dehydrogenase (SDH; Complex II), cytochrome c oxidase (COX; Complex IV), ATP syntase (Complex V) and cytochrome c. Anti-beta-actin antibody (b-Actin) was used as loading control. (B) Enzyme histochemical staining for Complex II (SDH) and complex IV (COX) activities. Complex II staining (SDH) remains unaltered in OPA1-deficient cells (-/-). In contrast, wild-type cells (+/+) with complex IV activity (COX) turned brown while OPA deficient cells remained unstained, showing no activity of complex IV. Scale bars: 10 μ m.

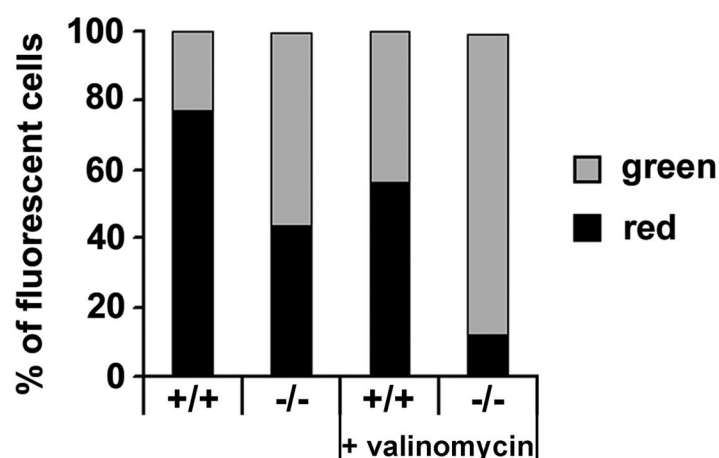


Figure 22. OPA1-deficient mouse embryonic fibroblasts show reduced membrane potential

Membrane potential measurements ($\Delta\Psi_m$) of MEFs. Cells were stained with JC-1. Percentages of green (grey) and red (black) fluorescent wild-type (+/+) and OPA1-deficient (-/-) cells are presented as bars. OPA1^{-/-} cells with normal $\Delta\Psi_m$ were much reduced in numbers. Addition of valinomycin led to a dissipation of $\Delta\Psi_m$ in OPA1^{-/-} cells and in wt MEFs. Red: normal $\Delta\Psi_m$. Green: reduced $\Delta\Psi_m$.

3.4.8. Cells deprived of OPA1 are less sensitive to staurosporine-induced apoptosis

Mitochondria of OPA1^{-/-} cells display severe abnormalities including fragmentation and loss of fusion (Figure 27), ultrastructural changes and cristae loss, respiration deficiency and membrane potential reduction. These kinds of changes have been lately connected to apoptosis. Thus, OPA1^{+/+}, OPA1^{+/-} and OPA1^{-/-} MEFs were exposed to intrinsic (staurosporine) and extrinsic (Tumor necrosis factor- α , TNF- α) apoptotic stimuli, to test their susceptibility to such reagents (Boatright and Salvesen, 2003). The intrinsic pathway is mitochondria-dependent; it is used to eliminate cells in response to ionising radiation, chemotherapeutic drugs (like staurosporine), mitochondrial damage and certain developmental cues. The extrinsic pathway is cytochrome c-independent; it is used for the elimination of unwanted cells during development, protection against transformed cells by the immune system, etc. Extrinsic factors, also called 'death-ligands', have a direct link to the apoptotic machinery (Ashkenazi and Dixit, 1998). They bind to death-receptors on the

plasma membrane and can activate caspases within seconds. As expected, lack of OPA1 did not affect cytochrome c-independent apoptotic pathways induced by TNF- α (Table 6). In contrast, OPA1^{-/-} cells unexpectedly proved to be less susceptible to staurosporine treatment. Four hours of staurosporine treatment drove 34% of wild-type, 35% of heterozygous, but only 10% of OPA1^{-/-} cells into programmed cell death (Figure 23A and Table 6). After 24 hours, most of the wild-type cells (91%) had died by apoptosis, compared to only 36% of cells lacking OPA1. In the intrinsic apoptotic pathway, mitochondria release cytochrome c that activates procaspase 9 by binding to Apaf1. Cytochrome c, Apaf1 and caspase 9 form a complex called the apoptosome (Figure 4), which further activates caspase 3 and finally culminates in apoptosis (Green and Reed, 1998). Broad caspase inhibitors, such as z-VAD-fmk, block all caspases including those activated by cytochrome c. z-VAD-fmk was used here to block caspases in MEFs prior to treatment with staurosporine. Apoptosis was blocked in OPA1^{+/+} MEFs in these experiments, resulting in a reduction of apoptotic cells to only 10% after 4 hours and to 35% after 24 hours of staurosporine treatment. This indicated that early apoptosis in OPA1^{+/+} MEFs was, indeed, induced by caspases which could be blocked by z-VAD-fmk. In OPA1^{-/-} MEFs the addition of z-VAD-fmk did not alter the response to staurosporine: after 4 hours only 10% and after 24h 35% of the cells had died. This means that caspases were not activated after staurosporine treatment in the OPA1^{-/-} cells. It seemed as if a block of cytochrome c release from the mitochondria prevented the activation of caspase-mediated cell death. In order to test this idea, mouse embryonic fibroblasts were again treated with staurosporine and stained with cytochrome c antibody. After 3 h of staurosporine treatment, 20% of wild-type cells showed release of cytochrome c. In contrast, OPA1 knockout cells retained cytochrome c in mitochondria as seen in untreated cells (Figure 23C). These results indicated that functional OPA1 is necessary for cytochrome c release induced by staurosporine during the early onset of apoptosis.

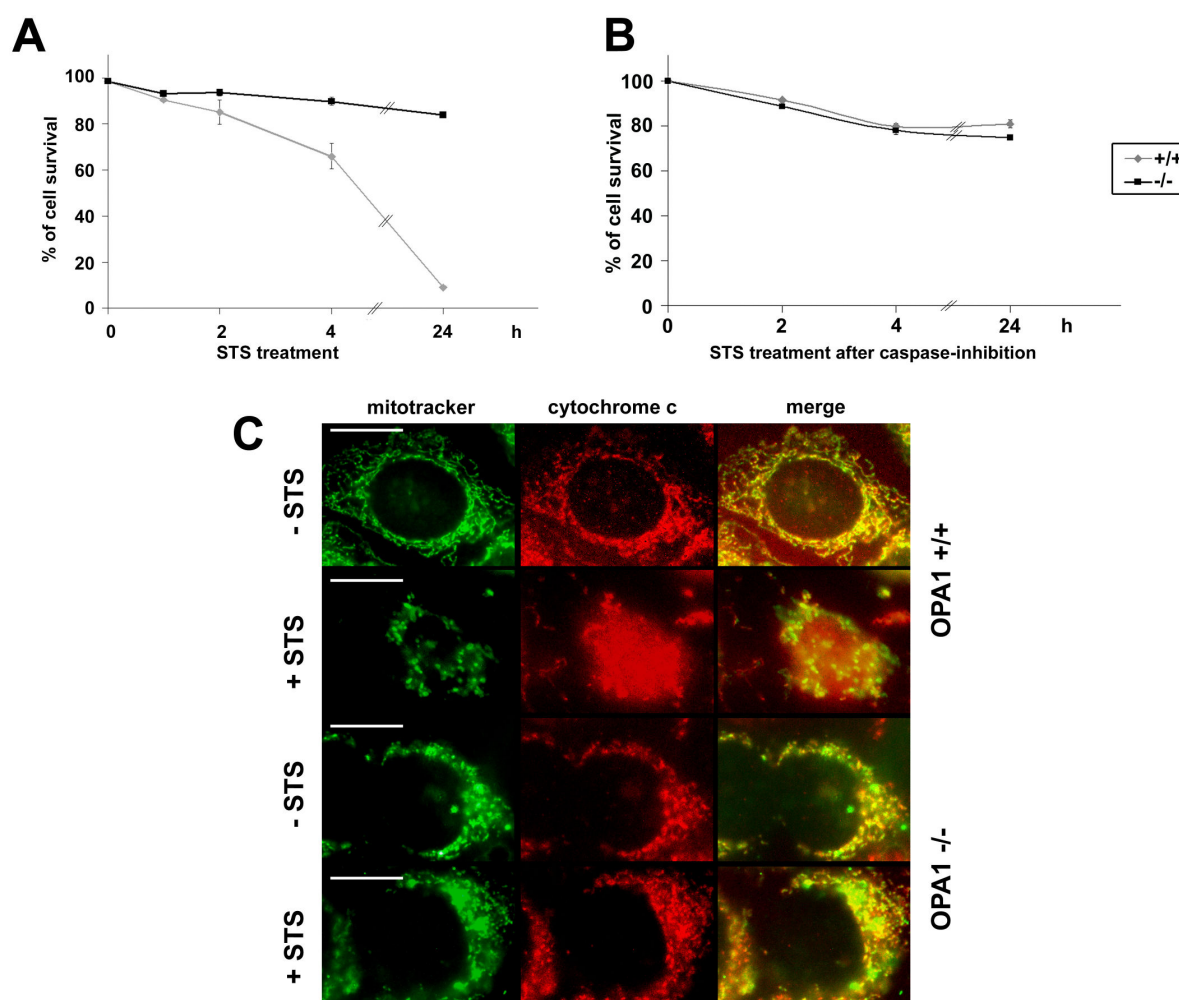


Figure 23. OPA1-deficient cells display reduced sensitivity to staurosporine-induced apoptosis

Survival rate of wild-type (+/+) and OPA1-deficient (-/-) cells after treatment with 2 μ M staurosporine for the indicated time without (A) or with an addition of 40 μ M of broad caspase-inhibitor z-VAD-fmk (B). n= 10. All bars indicate mean \pm SD. (C) Fluorescence microscopy using MitoTracker Green (left panel) and cytochrome c antibody (middle panel) on fibroblasts of indicated genotypes. Cells were first treated for 1 h with 100 nM z-VAD-fmk, and then with 2 μ M staurosporine (indicated as +STS) or left untreated (indicated as -STS). Right panel represents merged left and middle panel. All cells except for treated wild-type cells show mitochondrial localisation of cytochrome c. Wild-type cells show release of cytochrome c after 3 h of staurosporine treatment (OPA1^{+/+} +STS), but mutant cells after the same treatment (OPA1^{-/-} +STS) behave as untreated cells (OPA1^{-/-} -STS). Scale bars: 10 μ m.

Table 6. Percentage of OPA1 wild-type, heterozygous and homozygous knockout mouse embryonic fibroblasts that have undergone apoptosis after 4 and 24 hours of different treatments

		APOPTOSIS					
MEFs		OPA1 ^{+/+}	OPA1 ^{+/-}	OPA1 ^{-/-}	OPA1 ^{+/+}	OPA1 ^{+/-}	OPA1 ^{-/-}
treatment							
STS		34%	35%	10%	91%	90%	35%
STS + z-VAD-fmk		10%	NA	10%	35%	NA	34%
TNF α		5	NA	6%	22%	NA	24%

*NA stands for not analysed

3.4.9. OPA1 isoform 1 rescued the severe mitochondrial phenotype seen in OPA1 knockout cells

OPA1 knockout MEFs were retrovirally transduced with the mouse homologue of human *OPA1* isoform 1. In these cells, in contrast to untransduced knockout cells, elongated mitochondrial morphology was restored (Figure 27). In order to test the potential of this isoform to rescue other aspects of mitochondrial integrity, respiration efficiency, membrane potential and apoptosis susceptibility were assayed.

The functionality of respiratory chain complex IV was completely retrieved indicated by the brown colour development comparable to wild-type cells (Figure 24A). In addition, the membrane potential was also completely recovered to wild-type values (Figure 24B). These results indicate that isoform 1 is involved tubulation of mitochondria, that it is important for the function of respiratory chain complex IV and that it is required for maintenance of the mitochondrial membrane potential. In contrast to these results, OPA1 isoform 1 transduction of OPA1^{-/-} MEFs had no effect on their response towards staurosporine. After 4 h 12% and after 24 h only 36% of the OPA1 isoform 1-transduced cells had died, similar to the OPA1^{-/-} cells (Figure 24C).

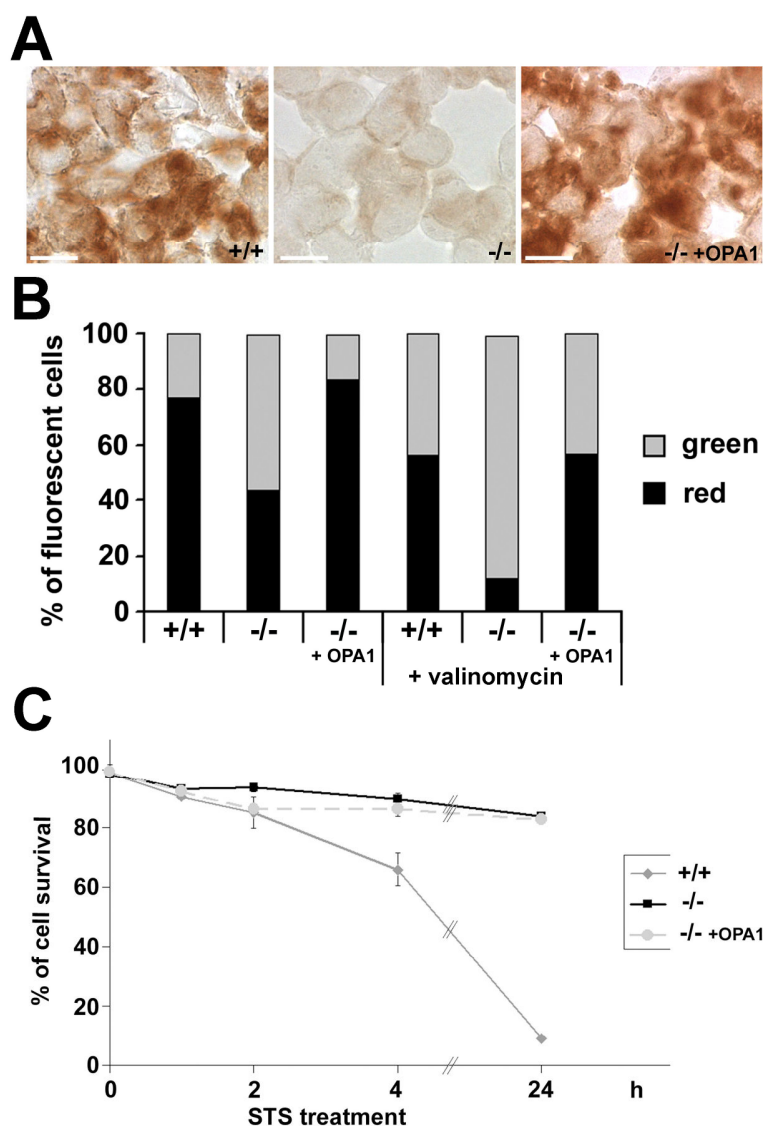


Figure 24. Analysis of rescued OPA1-null mouse embryonic fibroblasts

(A) Enzyme histochemical staining for complex IV activities. Wild-type cells (+/+) show complex IV activity brown staining while OPA1-deficient cells (-/-) remained unstained, same as in Figure 21B. Mutant cells transfected with OPA1-isoform 1 (-/- +OPA1) show rescued complex IV activity and retrieve brown staining. Scale bars: 10 μ m. (B) Membrane potential measurements ($\Delta\psi_m$) of MEFs. Cells were stained with JC-1. Percentages of green (grey) and red (black) fluorescent wild-type (+/+), OPA1-deficient cells (-/-) and OPA1-deficient cells transfected with OPA1-isoform 1 (-/- +OPA1) are presented as bars. OPA1^{-/-} cells showed reduced membrane potential, same as in Figure 22. OPA1^{-/-} cells transfected with OPA1-isoform 1 retrieved a normal membrane potential as seen in wild-type cells. (C) Survival rate of wild-type (+/+), OPA1-deficient cells (-/-) (both same as in Figure 23A) and OPA1-deficient cells transfected with OPA1-isoform 1 (-/-+OPA1) after treatment with 2 μ M staurosporine for the indicated time. OPA1 isoform 1 was not able to retrieve sensitivity to staurosporine observed for wild-type cells.